PERGAMON Computers and Mathematics with Applications 41 (2001) 735–756

An International Journal
computers & mathematics with applications

www.elsevier.nl/locate/camwa

# Goal-Oriented Error Estimation and Adaptivity for the Finite Element Method

J. T. ODEN* AND S. PRUDHOMME
Texas Institute for Computational and Applied Mathematics
The University of Texas at Austin
Austin, TX 78712, U.S.A.

*(Received and accepted August 1999)*

**Abstract**—In this paper, we study a new approach in *a posteriori* error estimation, in which the numerical error of finite element approximations is estimated in terms of quantities of interest rather than the classical energy norm. These so-called quantities of interest are characterized by linear functionals on the space of functions to where the solution belongs. We present here the theory with respect to a class of elliptic boundary-value problems, and in particular, show how to obtain accurate estimates as well as upper and lower bounds on the error. We also study the new concept of goal-oriented adaptivity, which embodies mesh adaptation procedures designed to control error in specific quantities. Numerical experiments confirm that such procedures greatly accelerate the attainment of local features of the solution to preset accuracies as compared to traditional adaptive schemes based on energy norm error estimates. 

**Keywords**—Goal-oriented error estimation, Quantities of interest, Error control, Mesh adaptivity, Upper and lower bounds.

## 1. INTRODUCTION

In recent years, a new approach to *a posteriori* error estimation has emerged for which the numerical error is estimated and controlled in terms of so-called quantities of interest. We shall refer to this approach as *goal-oriented error estimation* as the error is now measured with respect to a specific goal of the analysis instead of in the classical energy norm. Several methodologies have been advanced in [1–7]. This paper is a continuation of our earlier work [8] in which we presented the general theory as well as numerical experiments for the case of a two-point boundary value problem. In particular, we study here the quality of these error estimates for two-dimensional applications.

The quantities of interest represent physical quantities of the solution such as averages, flow rates, velocities, or shear stress at a point. Mathematically, these are characterized by linear functionals on the space of functions to which the solution belongs. The objective in goal-oriented error estimation is to relate the residual, the source of error, to the error in the quantity of interest. This involves the computation of an *influence function*, with respect to the linear

*Author to whom all correspondence should be addressed.
The support of this work by the Office of Naval Research under Contract N00014-95-1-0401 is gratefully acknowledged.

0898-1221/01/$ - see front matter  Typeset by AMS-TEX
PII: S0898-1221(00)00317-5

functional, given as the solution of the adjoint of the primal problem. The role played by the influence function is to indicate how the information is propagated from the residual to the error for the specific measure.

One attractive feature of the methodology is that the error estimates are given in terms of classical energy norm estimates of the errors in the numerical solution and numerical influence function. Reliable and accurate techniques have been developed to date to estimate the error in the global energy norm, using either residual methods (see [9–14]) or recovery methods (see [15,16]). We also describe how to estimate lower and upper bounds of the error in the goal. A natural adjunct to this new error estimation approach is goal-oriented adaptivity, where mesh adaptation is designed to accelerate the rate of convergence of the solution with respect to the quantity of interest.

Following the introduction, we present in Section 2 a model problem and relevant notations. The presentation of the theory of goal-oriented error estimation follows in detail in Section 3. We briefly describe, in Section 4, the methodology to derive lower and upper bounds on the error in the energy norm needed for our goal-oriented error estimates. We propose, in Section 5, an adaptation strategy to control the error in the quantity of interest. Finally, the method is applied to a two-dimensional boundary value problem with the numerical results recounted in Section 6, followed by a summary of our major conclusions.

## 2. MODEL PROBLEM AND NOTATION

Let $\Omega$ be an open bounded domain of $\mathbb{R}^d$ with Lipschitz boundary $\partial\Omega$. We consider the model boundary value problem which consists of finding the solution $u$ of

$$-\Delta u + cu = f, \qquad \text{in } \Omega \tag{2.1}$$

subject to the boundary conditions

$$\frac{\partial u}{\partial n} = g, \qquad \text{on } \Gamma_n \tag{2.2}$$

and

$$u = 0, \qquad \text{on } \Gamma_d. \tag{2.3}$$

The prescribed data is assumed to be smooth, in particular $f \in L^2$, $c$ is a nonnegative constant, $g \in L^2(\Gamma_n)$. The boundaries $\Gamma_d$ and $\Gamma_n$ are such that $\Gamma_d \cap \Gamma_n = \emptyset$, $\overline{\Gamma}_d \cup \overline{\Gamma}_d = \partial\Omega$, and we assume here that $\operatorname{meas} \Gamma_d > 0$.

The corresponding variational form of this problem is to find $u \in V$ such that

$$B(u,v) = F(v), \qquad \forall v \in V, \tag{2.4}$$

where $V$ is the Hilbert space

$$V = \{v \in H^1;\ v = 0,\ \text{on } \Gamma_d\} \tag{2.5}$$

and where

$$B(u,v) = \int_\Omega (\nabla u \cdot \nabla v + cuv)\, dx, \tag{2.6}$$

$$F(v) = \int_\Omega fv\, dx + \int_{\Gamma_n} gv\, ds. \tag{2.7}$$

The bilinear form $B(\cdot,\cdot)$ is symmetric positive-definite on $V \times V$, and therefore, defines an inner product on $V$. It is associated with the *energy norm*

$$\|v\|_e = \sqrt{B(v,v)}. \tag{2.8}$$

From the Lax-Milgram Theorem, we know that problem (2.4) admits a unique solution $u \in V$.

In order to approximate the solution $u$, one may construct a finite element space $V^{h,p} \subset V$ of hierarchical piecewise polynomial functions, where $h$ and $p$ refer to the size and maximal degree of the shape functions for each element, respectively (see, e.g., [17]). The mesh, formed by the union of all elements, is assumed to coincide exactly with $\Omega$. Using the classical Galerkin method, the finite element approximation $u_{h,p} \in V^{h,p}$ is the solution of

$$B(u_{h,p}, v) = F(v), \qquad \forall v \in V^{h,p}. \tag{2.9}$$

The numerical error in the approximation $u_{h,p}$ of $u$ is naturally defined as the function $e \in V$ such that

$$e = u - u_{h,p}. \tag{2.10}$$

Replacing $u$ by $(u_{h,p} + e)$ in (2.4), the error is shown to be governed by the equation

$$B(e, v) = \mathcal{R}^u_{h,p}(v), \qquad \forall v \in V, \tag{2.11}$$

where $\mathcal{R}^u_{h,p}$ denotes the *residual*

$$\mathcal{R}^u_{h,p}(v) = F(v) - b(u_{h,p}, v), \qquad v \in V. \tag{2.12}$$

The residual is a linear functional of the dual space $V'$ which depends on the data and the finite element solution $u_{h,p}$. It can be interpreted as the source of error as it is simply the source term in (2.11).

We immediately notice from (2.9) and (2.12) that the residual $\mathcal{R}^u_{h,p}(v)$ vanishes for all $v \in V^{h,p}$, i.e.,

$$\mathcal{R}^u_{h,p}(v) = 0, \qquad \forall v \in V^{h,p}. \tag{2.13}$$

Using (2.11), this yields the well-known *orthogonality property* (with respect to the inner product $B(\cdot, \cdot)$),

$$B(e, v) = 0, \qquad \forall v \in V^{h,p}. \tag{2.14}$$

The principal goal in *a posteriori* error estimation is to postprocess the residual in order to derive, in an inexpensive manner, relevant measures of the error.

## 3. GOAL-ORIENTED ERROR ESTIMATION

The object of goal-oriented error estimation is to assess the accuracy of finite element solutions in measures other than the classical energy norm. In the following, we review the general approach assuming the measure can be characterized as a linear functional on the solution space. We then propose several examples of functionals of potential interest.

### 3.1. General Approach

Let $L$ denote a bounded linear functional in $V'$ and let us suppose that the goal of the computations is the evaluation of the quantity $L(u)$. Then, the accuracy of $L(u_{h,p})$ is assessed in terms of the error $\mathcal{E}^L \in \mathbb{R}$, which reads, due to the linearity of $L$,

$$\mathcal{E}^L = L(u) - L(u_{h,p}) = L(u - u_{h,p}) = L(e). \tag{3.1}$$

One possible way to evaluate $\mathcal{E}^L$ would be to approximate the error $e$ using (2.11) and then to compute $\mathcal{E}^L = L(e)$. However, problem (2.11) for the error is, of course, generally too expensive to solve numerically. The alternative approach is to relate $L(e)$ to the residual $\mathcal{R}^u_{h,p}$ without having to compute the error $e$. Such an approach is justified since the residual contains all the information which drives the numerical error.

Hence, the starting point is to find the relationship between the quantity $L(e)$ and the source of error $\mathcal{R}^u_{h,p}$; namely, we would like to find a linear functional $\omega$, if one exists, such that

$$L(e) = \omega\left(\mathcal{R}^u_{h,p}\right). \tag{3.2}$$

We shall refer to $\omega$ as the *influence function* with respect to $L$, as it indicates the influence of the residual on $L(e)$. At this stage, we recognize that $\omega$ is an element of the bidual of $V$, and since $V$ was assumed a Hilbert space, and *a fortiori* a reflexive space, (3.2) becomes

$$L(e) = \mathcal{R}^u_{h,p}(\omega), \tag{3.3}$$

where $\omega$ is now identified with an element of $V$.

We now show how to derive the influence function. Using (2.11) and (3.3), we immediately obtain

$$L(e) = B(e, \omega). \tag{3.4}$$

The equality above is necessarily verified when $\omega \in V$ is the solution of

$$B(v, \omega) = L(v), \qquad \forall v \in V. \tag{3.5}$$

This problem has often been referred to as the *adjoint* or *dual problem* (see, e.g., [18]) of the primal problem (2.4). The *Lax-Milgram Theorem* allows us to conclude the existence and uniqueness of $\omega$ in $V$.

LEMMA 3.1. *Let $\omega_{h,p} \in V^{h,p}$ be a finite element approximation of $\omega$ such that*

$$B(v, \omega_{h,p}) = L(v), \qquad \forall v \in V^{h,p}. \tag{3.6}$$

*Then*

$$L(e) = B(e, \varepsilon), \tag{3.7}$$

*where $\varepsilon \in V$ denotes the numerical error in $\omega_{h,p}$, namely $\varepsilon = \omega - \omega_{h,p}$.*

PROOF. From the orthogonality property (2.14), we have

$$B(e, \omega_{h,p}) = \mathcal{R}^u_{h,p}(\omega_{h,p}) = 0. \tag{3.8}$$

And combining (3.4) and (3.8), we get

$$L(e) = B(e, \omega) - B(e, \omega_{h,p}) = B(e, \omega - \omega_{h,p}) = B(e, \varepsilon), \tag{3.9}$$

as asserted. We remark from (3.8) that the approximation $\omega_{h,p}$ fails to provide any valuable information on $L(e)$. ∎

For the model problem considered here, the bilinear form $B(\cdot, \cdot)$ defines an inner product on $V \times V$ with associated norm $\|\cdot\|_e$. A new relationship for $L(e)$ has been suggested by Babuška [7] as the following.

THEOREM 3.1. *Under the foregoing definitions and assumptions,*

$$L(e) = B(e, \varepsilon) = \frac{1}{4}\|e + \varepsilon\|_e^2 - \frac{1}{4}\|e - \varepsilon\|_e^2. \tag{3.10}$$

PROOF. We note that

$$\|e + \varepsilon\|_e^2 = B(e + \varepsilon, e + \varepsilon) = B(e, e) + 2B(e, \varepsilon) + B(\varepsilon, \varepsilon), \tag{3.11}$$

$$\|e - \varepsilon\|_e^2 = B(e - \varepsilon, e - \varepsilon) = B(e, e) - 2B(e, \varepsilon) + B(\varepsilon, \varepsilon). \tag{3.12}$$

Combining these two results, we have

$$\|e+\varepsilon\|_e^2 - \|e-\varepsilon\|_e^2 = 4B(e,\varepsilon), \tag{3.13}$$

which provides, with Lemma 3.1, the relation to be proved. ∎

We propose a modified version of (3.10) using a scaling factor $s \in \mathbb{R}$,

$$L(e) = B(e,\varepsilon) = B\left(se, \frac{\varepsilon}{s}\right) = \frac{1}{4}\left\|se + \frac{\varepsilon}{s}\right\|_e^2 - \frac{1}{4}\left\|se - \frac{\varepsilon}{s}\right\|_e^2. \tag{3.14}$$

The value of $s$ is chosen so that the quantities $\|se\|_e$ and $\|\varepsilon/s\|_e$ have same amplitudes, i.e., $\|se\|_e = \|\varepsilon/s\|_e$, which implies that

$$s = \sqrt{\frac{\|\varepsilon\|_e}{\|e\|_e}}. \tag{3.15}$$

Such a choice of $s$ is justified because it minimizes the quantities $\|se + \varepsilon/s\|_e^2$ and $\|se - \varepsilon/s\|_e^2$. Moreover, the scaler $s$ ensures the *scalability* of relationship (3.14). If we multiply the load $F$ in the original problem by a factor $a$, the term on the right-hand side of (3.14) just needs to be multiplied by $a$ to obtain the new error $L(e)$. This result is not true in the case of (3.10).

### 3.2. Approximations and Bounds for the Error Quantity $L(e)$

Equation (3.14) establishes the relation between the error quantity $L(e)$ and energy norms of linear combinations of $e$ and $\varepsilon$. Let $\eta_{\text{low}}^+$, $\eta_{\text{upp}}^+$, $\eta_{\text{low}}^-$, and $\eta_{\text{upp}}^-$ denote global error estimates (we show in Section 4 how they are derived) such that

$$\eta_{\text{low}}^+ \le \left\|se + \frac{\varepsilon}{s}\right\|_e \le \eta_{\text{upp}}^+, \tag{3.16}$$

$$\eta_{\text{low}}^- \le \left\|se - \frac{\varepsilon}{s}\right\|_e \le \eta_{\text{upp}}^-. \tag{3.17}$$

It is then straightforward to derive the following estimates of $L(e)$:

$$L(e) \approx \eta_{\text{eel}}^L = \frac{1}{4}\left(\eta_{\text{low}}^+\right)^2 - \frac{1}{4}\left(\eta_{\text{low}}^-\right)^2, \tag{3.18}$$

$$L(e) \approx \eta_{\text{eeu}}^L = \frac{1}{4}\left(\eta_{\text{upp}}^+\right)^2 - \frac{1}{4}\left(\eta_{\text{upp}}^-\right)^2, \tag{3.19}$$

as well as the averaged estimate

$$L(e) \approx \eta_{\text{eea}}^L = \frac{1}{2}\left(\eta_{\text{eel}}^L + \eta_{\text{eeu}}^L\right). \tag{3.20}$$

THEOREM 3.2. LOWER AND UPPER BOUNDS. *Let the quantities $\eta_{\text{low}}^L$ and $\eta_{\text{upp}}^L$ be defined as*

$$\eta_{\text{low}}^L = \frac{1}{4}\left(\eta_{\text{low}}^+\right)^2 - \frac{1}{4}\left(\eta_{\text{upp}}^-\right)^2, \tag{3.21}$$

$$\eta_{\text{upp}}^L = \frac{1}{4}\left(\eta_{\text{upp}}^+\right)^2 - \frac{1}{4}\left(\eta_{\text{low}}^-\right)^2. \tag{3.22}$$

*Then, $\eta_{\text{low}}^L$ and $\eta_{\text{upp}}^L$ provide a lower and upper bound on $L(e)$,*

$$\eta_{\text{low}}^L \le L(e) \le \eta_{\text{upp}}^L. \tag{3.23}$$

*We note that the average of $\eta_{\text{low}}^L$ and $\eta_{\text{upp}}^L$ gives $\eta_{\text{eea}}^L$ as well.*

PROOF. Immediately follows from (3.14). ∎

REMARK 3.1. QUALITY OF THE BOUNDS AND ESTIMATES. We evaluate the quality of the bounds $\eta^L_{\text{low}}$ and $\eta^L_{\text{upp}}$ in terms of the effectivity indices of $\eta^+_{\text{low}}$, $\eta^+_{\text{upp}}$, $\eta^-_{\text{low}}$, and $\eta^-_{\text{upp}}$. Let the effectivity indices be

$$\lambda^-_{\text{low}} = \frac{\eta^-_{\text{low}}}{\|se - \varepsilon/s\|_e}, \qquad \lambda^-_{\text{upp}} = \frac{\eta^-_{\text{upp}}}{\|se - \varepsilon/s\|_e},$$
$$\lambda^+_{\text{low}} = \frac{\eta^+_{\text{low}}}{\|se + \varepsilon/s\|_e}, \qquad \lambda^+_{\text{upp}} = \frac{\eta^+_{\text{upp}}}{\|se + \varepsilon/s\|_e}.$$

Then, using (3.14) and assuming $L(e)$ different from zero, we have

$$\begin{aligned}\frac{\eta^L_{\text{low}}}{L(e)} &= \frac{1}{L(e)}\left(\frac{1}{4}\left(\eta^+_{\text{low}}\right)^2 - \frac{1}{4}\left(\eta^-_{\text{upp}}\right)^2\right)\\ &= \frac{1}{L(e)}\left(\frac{1}{4}\left(\lambda^+_{\text{low}}\right)^2\left\|se + \frac{\varepsilon}{s}\right\|_e^2 - \frac{1}{4}\left(\lambda^-_{\text{upp}}\right)^2\left\|se - \frac{\varepsilon}{s}\right\|_e^2\right)\\ &= \frac{1}{L(e)}\left(\frac{1}{4}\left(\lambda^+_{\text{low}}\right)^2\left\|se + \frac{\varepsilon}{s}\right\|_e^2 - \frac{1}{4}\left(\lambda^-_{\text{upp}}\right)^2\left\|se + \frac{\varepsilon}{s}\right\|_e^2 + \left(\lambda^-_{\text{upp}}\right)^2 L(e)\right),\end{aligned}$$

so the following effectivity index for the lower bound on $L(e)$ is given by

$$\lambda^L_{\text{low}} = \frac{\eta^L_{\text{low}}}{L(e)} = \left(\lambda^-_{\text{upp}}\right)^2 + \frac{1}{4}\left(\left(\lambda^+_{\text{low}}\right)^2 - \left(\lambda^-_{\text{upp}}\right)^2\right)\frac{\|se + \varepsilon/s\|_e^2}{L(e)}.$$

In the same manner, we have for the upper bound

$$\lambda^L_{\text{upp}} = \frac{\eta^L_{\text{upp}}}{L(e)} = \left(\lambda^-_{\text{low}}\right)^2 + \frac{1}{4}\left(\left(\lambda^+_{\text{upp}}\right)^2 - \left(\lambda^-_{\text{low}}\right)^2\right)\frac{\|se + \varepsilon/s\|_e^2}{L(e)}.$$

Therefore, the quality of the bounds directly depends on the ratio $\|se + \varepsilon/s\|_e^2/L(e)$. This ratio can take on large values depending on the quantity of interest. Also, when adaptivity aims at controlling $L(e)$ instead of $\|e\|_e$, this ratio may have a tendency to increase. As a consequence, in order to obtain effectivity indices $\lambda^L_{\text{low}}$ and $\lambda^L_{\text{upp}}$ close to one, the effectivity indices with respect to the quantities in the energy norm should be excellent, i.e., very close to one, so that $(\lambda^+_{\text{low}})^2 - (\lambda^-_{\text{upp}})^2$ and $(\lambda^+_{\text{upp}})^2 - (\lambda^-_{\text{low}})^2$ are close to zero. Otherwise, we may expect $\lambda^L_{\text{low}}$ and $\lambda^L_{\text{upp}}$ to deteriorate when the ratio becomes very large.

On the other hand, the effectivity index of the estimate $\eta^L_{\text{eel}}$ is given by

$$\lambda^L_{\text{eel}} = \frac{\eta^L_{\text{eel}}}{L(e)} = \left(\lambda^+_{\text{low}}\right)^2 + \frac{1}{4}\left(\left(\lambda^-_{\text{low}}\right)^2 - \left(\lambda^-_{\text{low}}\right)^2\right)\frac{\|se + \varepsilon/s\|_e^2}{L(e)}.$$

This time, the difference $(\lambda^+_{\text{low}})^2 - (\lambda^-_{\text{low}})^2$ is very close to zero as we expect the global error estimator to provide similar effectivity indices $\lambda^+_{\text{low}}$ and $\lambda^-_{\text{low}}$. Therefore, the quality of $\eta^L_{\text{eel}}$ should not depend on the ratio $\|se + \varepsilon/s\|_e^2/L(e)$, however large it may be. The same remark holds for the estimates $\eta^L_{\text{eeu}}$ and $\eta^L_{\text{eea}}$.

An alternative approach to derive bounds on the quantity $L(e)$ follows from relation (3.7) employing the Cauchy-Schwartz inequality

$$|L(e)| = |B(e,\varepsilon)| \le \sum_K |B_K(e,\varepsilon)| \le \sum_K \|e\|_{e,K}\|\varepsilon\|_{e,K}, \tag{3.24}$$

where $B_K(\cdot,\cdot)$ and $\|\cdot\|_{e,K}$ denote the restrictions of $B(\cdot,\cdot)$ and $\|\cdot\|_e$ on a element $\Omega_K$. Let $\eta^u$ and $\eta^\omega$ denote two global estimates of $\|e\|_e$ and $\|\varepsilon\|_e$. Since $\eta^u$ and $\eta^\omega$ can be decomposed into the contributions $\eta^u_K$ and $\eta^\omega_K$ for each element $\Omega_K$, we define

$$\eta^L_{\text{cs}} = \sum_K \eta^u_K\,\eta^\omega_K, \tag{3.25}$$

such that

$$|L(e)| \leq \sum_K \|e\|_{e,K} \|\varepsilon\|_{e,K} \approx \eta_{cs}^L. \tag{3.26}$$

This approach has been followed by Rannacher *et al.* [1–3] with the exception that they use explicit-type and interpolation-type error estimators to evaluate the local contributions $\|e\|_{e,K}$ and $\|\varepsilon\|_{e,K}$, respectively, for which unknown constants are introduced.

### 3.3. Examples of Bounded Linear Functionals

We provide here some examples of quantities of interest and characterize them in terms of bounded linear functionals. In finite element applications, it appears suitable to express the quantity of interest, if possible, in the form of an integral over the domain $\Omega$, since integration is at the heart of all finite element codes. Let us assume $V = H_0^1(\Omega)$ in what follows.

A quantity of possible interest is the average of the solution $u$ over a subdomain $\Omega_s \in \Omega$. The corresponding linear functional is written as

$$L(u) = \frac{1}{|\Omega_s|} \int_\Omega k(\mathbf{x})\, u(\mathbf{x})\, dx, \tag{3.27}$$

where $k(\mathbf{x})$ is equal to one if $\mathbf{x} \in \Omega_s$ and zero, otherwise, and where $|\Omega_s|$ defines the area or volume of $\Omega_s$.

PROPOSITION 3.1. *Let $u \in H_0^1(\Omega)$. Then, the linear functional $L(u) = \int_\Omega k\, u\, dx$ is bounded on $H_0^1(\Omega)$.*

PROOF. Since $u \in H_0^1(\Omega)$ and $k \in L^2(\Omega)$, we obtain, using Minkowski's inequality,

$$L(u) = \int_\Omega k\, u\, dx \leq \|k\|_0 \|u\|_0 \leq C_0\, |\Omega_s|\, |u|_1, \tag{3.28}$$

where $C_0$ is the Poincaré constant. ∎

When the solution is a vector-valued function in $(H_0^1(\Omega))^d$, one may be interested in the flux through $\partial\Omega_s$ of $\Omega_s$, in which case the functional reads

$$L(\mathbf{u}) = \int_{\partial\Omega_s} \mathbf{u} \cdot \mathbf{n}\, ds = \int_{\Omega_s} \nabla \cdot \mathbf{u}\, dx = \int_\Omega k(\mathbf{x})\, \nabla \cdot \mathbf{u}(\mathbf{x})\, dx. \tag{3.29}$$

This also defines a bounded linear functional.

It may happen that the goal is to evaluate nonlinear quantities $N(u)$ of the solution $u$ such as

$$N(u) = \int_{\Omega_s} u^2\, dx. \tag{3.30}$$

In that case, the error quantity $\mathcal{E}^L$ reads

$$\mathcal{E}^N = N(u) - N(u_{h,p}) = \int_{\Omega_s} u^2 - u_{h,p}^2\, dx = 2 \int_{\Omega_s} u_{h,p} e\, dx + \int_{\Omega_s} e^2\, dx. \tag{3.31}$$

Neglecting the higher-order term in $e$, we may consider the following linear functional, which is bounded:

$$L(e) = 2 \int_{\Omega_s} u_{h,p} e\, dx = 2 \int_\Omega k(\mathbf{x}) u_{h,p}(\mathbf{x}) e(\mathbf{x})\, dx \tag{3.32}$$

and apply the goal-oriented error estimation methodology described above in order to obtain an estimate of $\mathcal{E}^N \approx L(e)$.

However, there exist numerous other quantities of interest, which cannot be characterized by a bounded linear functional. In particular, this is the case for the value of the solution at a given point of the domain. This issue is addressed in the next section.

### 3.4. Extension to Pointwise Error Estimation

Pointwise error estimation aims at assessing the accuracy of the solution or quantity of the solution at a given point $\mathbf{x}_0 \in \overline{\Omega}$. Unfortunately, for $u \in H^1(\Omega)$, $\Omega \subset \mathbb{R}^d$, we know from the *Sobolev Embedding Theorem* that $u$ may not be defined at $\mathbf{x}_0$ when the geometrical dimension $d$ is equal or greater than two. In other words, the linear functional corresponding to the quantity of interest $u(\mathbf{x}_0)$,

$$L(u) = u(\mathbf{x}_0) \tag{3.33}$$

is not necessarily bounded.

We appeal here to the use of *mollification* (see [19, Chapter 2]) in order to circumvent this issue, which allows us to introduce the following functional:

$$L(u) = \langle u \rangle_\epsilon(\mathbf{x}_0) = \int_\Omega u(\mathbf{x})\, k_\epsilon(\mathbf{x} - \mathbf{x}_0)\, dx, \tag{3.34}$$

where the mollifiers $k_\epsilon$ form a family of infinitely smooth functions in $(-\infty, \infty)^d$ characterized by the parameter $\epsilon$. The quantity $\langle u \rangle_\epsilon(\mathbf{x}_0)$ is viewed as the average of $u$ over a small neighborhood of $\mathbf{x}_0$. The mollifiers $k_\epsilon$ are chosen here of the form

$$k_\epsilon(\mathbf{x}) = \begin{cases} C \exp\left( \dfrac{|\mathbf{x}|^2}{\epsilon^2} - 1 \right)^{-1}, & \text{if } |\mathbf{x}| < \epsilon, \\ 0, & \text{if } |\mathbf{x}| \geq \epsilon, \end{cases} \tag{3.35}$$

where the constant $C$, which depends on $d$, $\epsilon$, and $\mathbf{x}_0$, is selected to satisfy

$$\int_\Omega k_\epsilon(\mathbf{x} - \mathbf{x}_0)\, dx = 1. \tag{3.36}$$

As a remark, we note that it is not necessary to employ so smooth mollifiers to obtain a bounded linear functional on $H^1(\Omega)$.

Our motivation to use mollification procedure relies on the following properties. When $u \in L^2(\Omega)$, the function $\mathbf{x}_0 \longmapsto \langle u \rangle_\epsilon(\mathbf{x}_0)$ converges to $u$ when $\epsilon$ tends to zero. Moreover, when $u$ is constant or linear in the ball $\mathcal{B}(\mathbf{x}_0, \epsilon) \subset \Omega$, we have $\langle u \rangle_\epsilon(\mathbf{x}_0) = u(\mathbf{x}_0)$ independently of the value of $\epsilon$.

REMARK 3.2. NUMERICAL INTEGRATION. In order to compute $L(u)$ in (3.34) and the constant $C$ in (3.36), it is necessary to perform a numerical integration of the mollifiers $k_\epsilon$. These functions are very local in nature, and because integration is generally carried out using classical Gauss quadrature rules, it appears necessary to limit the size of the support of $k_\epsilon(\mathbf{x} - \mathbf{x}_0)$, equal to $2\epsilon$, with respect to the mesh size $h$ of the element containing the point $\mathbf{x}_0$. Therefore, one requires that

$$\kappa \leq \frac{2\epsilon}{h}, \tag{3.37}$$

where $\kappa$ is a given fractional number, $0 < \kappa \leq 1$. In order to attain an acceptable accuracy for $L$ while avoiding too many Gaussian points, we have suggested the value $\kappa = 1/4$ in [8].

This approach also applies to estimate the pointwise error in directional derivatives of the solution. We then consider the bounded linear functional

$$L(u) = \langle \mathbf{n} \cdot \nabla u \rangle_\epsilon(\mathbf{x}_0) = \int_\Omega \mathbf{n} \cdot \nabla u(\mathbf{x})\, k_\epsilon(\mathbf{x} - \mathbf{x}_0)\, dx, \tag{3.38}$$

where $\mathbf{n}$ is the unit vector representing the direction of interest.

# 4. ERROR ESTIMATION IN ENERGY NORM

In the present section, we briefly analyze the methodology to obtain global lower and upper bounds on the error in the energy norm to be utilized in goal-oriented error estimation. We recall that the error $e$ in the numerical solution $u_{h,p}$ is governed by

$$B(e,v) = \mathcal{R}^u_{h,p}(v) = F(v) - B(u_{h,p},v), \qquad \forall v \in V, \tag{4.1}$$

whereas the error $\varepsilon$ in the finite element approximation $\omega_{h,p}$ of the influence function satisfies

$$B(v,\varepsilon) = \mathcal{R}^w_{h,p}(v) = L(v) - B(v,\omega_{h,p}), \qquad \forall v \in V. \tag{4.2}$$

In what follows, the error estimates are presented with respect to the error $e$ only as the results straightforwardly apply to $\varepsilon$.

The objective is to estimate the quantity $\|e\|_e$ by the residual approach. Introducing the norm of the residual in the dual space $V'$ as

$$\left\|\mathcal{R}^u_{h,p}\right\|_* = \sup_{v\in V\setminus\{0\}} \frac{\left|\mathcal{R}^u_{h,p}(v)\right|}{\|v\|_e}, \tag{4.3}$$

the error can be related to the residual as follows.

THEOREM 4.3. *Let $e \in V$ be the error in the approximation $u_{h,p}$ of the exact solution of problem (2.4) and let $\mathcal{R}^u_{h,p} \in V'$ denote the residual as defined in (4.1). Then*

$$\|e\|_e = \left\|\mathcal{R}^u_{h,p}\right\|_* . \tag{4.4}$$

PROOF. Replacing $v$ by $e$ in (4.1), we have

$$\|e\|_e^2 = B(e,e) = \mathcal{R}^u_{h,p}(e) \le \left\|\mathcal{R}^u_{h,p}\right\|_* \|e\|_e,$$

which shows that $\|e\|_e \le \|\mathcal{R}^u_{h,p}\|_*$. Next, we show that $\|\mathcal{R}^u_{h,p}\|_* \le \|e\|_e$. From the definition of the norm of the residual, using equation (4.1) and the Cauchy-Schwartz inequality, we get

$$\left\|\mathcal{R}^u_{h,p}\right\|_* = \sup_{v\in V\setminus\{0\}} \frac{|\mathcal{R}^u_{h,p}(v)|}{\|v\|_e} = \sup_{v\in V\setminus\{0\}} \frac{|B(e,v)|}{\|v\|_e} \le \sup_{v\in V\setminus\{0\}} \frac{\|e\|_e\,\|v\|_e}{\|v\|_e} \le \|e\|_e,$$

which completes the proof of the theorem. ∎

Thus, the *energy norm* represents the *optimal* norm in which the error can be estimated using the information provided by the residual. Unfortunately, the norm of the residual is not readily computable. In fact, using the *Riesz Representation Theorem*, there exists a unique function $\varphi \in V$ which satisfies

$$\left\|\mathcal{R}^u_{h,p}\right\|_* = \|\varphi\|_e \tag{4.5}$$

and

$$B(\varphi,v) = \mathcal{R}^u_{h,p}(v), \qquad \forall v \in V. \tag{4.6}$$

Since problems (4.1) and (4.6) are identical and because their solutions are known to be unique, we conclude that $\varphi = e$. We, nevertheless, retain the notation $\varphi$ since the functions $\varphi$ and $e$ may be different for problems which are not symmetric positive definite. Note that problem (4.6) is infinite dimensional, which implies that only approximations of $\varphi$ can be obtained. The objective is then to postprocess the residual in a efficient manner in order to derive lower and upper bounds on $\|e\|_e$, i.e., $\|\mathcal{R}^u_{h,p}\|_*$. This may be achieved by constructing two adequate spaces $V_-$ and $V_+$, $V_- \subseteq V \subseteq V_+$, so that

$$\sup_{v\in V_-\setminus\{0\}} \frac{\left|\mathcal{R}^u_{h,p}(v)\right|}{\|v\|_e} \le \left\|\mathcal{R}^u_{h,p}\right\|_* \le \sup_{v\in V_+\setminus\{0\}} \frac{\left|\mathcal{R}^u_{h,p}(v)\right|}{\|v\|_e} \tag{4.7}$$

provided that one can find a proper extension of $\mathcal{R}^u_{h,p}$ to the space $V_+$.

### 4.1. Upper Bound for the Error in the Energy Norm

We present here the outlines of the methodology proposed by Ainsworth and Oden [10]. Let $\mathcal{P}^h$ denote a partition of $\Omega$ into the elements $\Omega_K$, $K = 1, \ldots, N_e$. It is convenient to consider the local spaces $V_K$ for each element $\Omega_K \in \mathcal{P}^h$ as

$$V_K = \left\{ v_K \in H^1(\Omega_K);\ v_K = 0,\ \text{on } \Gamma_d \cap \partial\Omega_K \right\}. \tag{4.8}$$

Then, we introduce the *broken space* $V(\mathcal{P}^h)$ as

$$V\left(\mathcal{P}^h\right) = \left\{ v \in L^2(\Omega); v_K = v|_K \in V_K,\ \forall \Omega_K \in \mathcal{P}^h \right\}. \tag{4.9}$$

It is important to observe that $V \subset V(\mathcal{P}^h)$.

We denote the restrictions of the forms $B(\cdot,\cdot)$ and $\mathcal{R}^u_{h,p}(\cdot)$ on an element $\Omega_K$ of the partition by

$$B_K(u_K, v_K) = \int_{\Omega_K} \nabla u_K \nabla v_K + c u_K v_K \, dx, \tag{4.10}$$

$$\mathcal{R}^u_{h,p,K}(v_K) = \int_{\Omega_K} f|_K v_K \, dx - \int_{\Omega_K} \nabla u_{h,p}|_K \nabla v_K + c u_{h,p}|_K v_K \, dx. \tag{4.11}$$

Then, extensions of the residual $\mathcal{R}^u_{h,p}$ to the whole space $V(\mathcal{P}^h)$ are given by

$$\hat{\mathcal{R}}^u_{h,p}(v) = \sum_K \left[ \mathcal{R}^u_{h,p,K}(v|_K) + \oint_{\partial\Omega_K} g_K v|_K \, ds \right], \tag{4.12}$$

where the arbitrary functions $g_K$ must satisfy the condition

$$\sum_K \oint_{\partial\Omega_K} g_K v|_K \, ds = 0, \qquad \forall v \in V. \tag{4.13}$$

For example, the condition above holds if we choose $g_K = 0$ on each element edge lying on $\partial\Omega$ and if we choose $g_K + g_J = 0$ for each interior edge common to two elements $\Omega_K$ and $\Omega_J$.

THEOREM 4.4. UPPER BOUND. *For each element $\Omega_K \in \mathcal{P}^h$, let $\varphi_K \in V_K$ denote the solution of*

$$B_K(\varphi_K, v_K) = \mathcal{R}^u_{h,p,K}(v_K) + \oint_{\partial\Omega_K} g_K v_K \, ds, \qquad \forall v_K \in V_K. \tag{4.14}$$

*Then*

$$\|e\|_e = \left\|\mathcal{R}^u_{h,p}\right\|_* \le \sqrt{\sum_K \|\varphi_K\|^2_{e,K}} = \sqrt{\sum_K B_K(\varphi_K, \varphi_K)}. \tag{4.15}$$

PROOF. See [10,20]. ∎

The dimension of the spaces $V_K$ is infinite, so the local problems (4.14) are, at best, approximated in local finite element spaces. For instance, instead of (4.14), we solve for $\tilde{\varphi}_K \in \tilde{V}^{h,p}_K$ such that

$$B_K(\tilde{\varphi}_K, v_K) = \mathcal{R}^u_{h,p,K}(v_K) + \oint_{\partial\Omega_K} g_K v_K \, ds, \qquad \forall v_K \in \tilde{V}^{h,p}_K, \tag{4.16}$$

where $\tilde{V}^{h,p}_K$ is the discrete space $V^{h,p}_K$ augmented by the addition of polynomials of degree up to $p+q$, $q > 0$ (we shall use $q = 2$ in the numerical experiments). The functions $g_K$ are determined by the *equilibrated flux splitting* method, as described in [10]. They are constructed using piecewise linear functions on each edge and by enforcing the *equilibration condition*

$$\mathcal{R}^u_{h,p,K}(1) + \oint_{\partial\Omega_K} g_K \, ds = 0. \tag{4.17}$$

This condition is actually necessary when $c = 0$ to ensure the solvability of the local problems (4.16).

We finally denote $\eta^u_{\text{upp}}$ the error estimate in the energy norm

$$\eta^u_{\text{upp}} = \sqrt{\sum_K \|\tilde{\varphi}_K\|^2_{e,K}} = \sqrt{\sum_K B_K(\tilde{\varphi}_K, \tilde{\varphi}_K)}. \tag{4.18}$$

The quantity $\eta^u_{\text{upp}}$ is not guaranteed to provide an upper bound on $\|e\|_e$ due to the approximation $\tilde{\varphi}_K$ of $\varphi_K$. However, the numerical experiments will show that $\eta^u_{\text{upp}}$ is an upper bound when $h$ is sufficiently small.

### 4.2. Lower Bound for the Error in the Energy Norm

In order to obtain a lower bound, we have seen that it is necessary to determine a vector space $V_- \subset V$. Let $W$ be the finite element space, commonly called the space of perturbations, constructed as

$$W \neq \{0\}, \qquad W \cap V^{h,p} = \{0\}, \qquad W \cup V^{h,p} \subset V. \tag{4.19}$$

THEOREM 4.5. LOWER BOUND. *Let $\psi \in W$ denote the solution of*

$$B(\psi, v) = \mathcal{R}^u_{h,p}(v), \qquad \forall v \in W. \tag{4.20}$$

*Then*

$$\|e\|_e = \left\|\mathcal{R}^u_{h,p}\right\|_* \geq \|\psi\|_e. \tag{4.21}$$

PROOF. The proof immediately follows from the fact that $\psi \in W \subset V$. ∎

The choice of $W$ is not unique. It is controlled by the *trade-off between cost and accuracy*. For high accuracy, it is desirable that $W$ contains many degrees of freedom, but this in turn would result in a prohibitively expensive problem (4.20). Here, $W$ is conveniently constructed from layers of piecewise polynomial basis functions involving polynomials of degree between $p+1$ and $p+q$, $q \geq 1$. These basis functions are commonly called the *bubble* functions. The distribution of $q$ over the elements is usually chosen to be uniform, i.e., $q = 1$ or 2, but we advocate an adaptative search for $q$. In two-dimensional problems, for example, the space $W$ can consist, as a first guess, of "edge" bubbles of degree $q = 1$. Then it can be successively enriched with "interior" and "edge" bubbles of higher degree in the elements where we have large contributions to the previous global estimates. Finally, in order to efficiently solve the global problem (4.20), we propose to use the conjugate-gradient method performing only a few iterations. The quality of this lower bound depends on the "richness" of $W$, that is on the value of $q$, and on the fact that the spaces $W$ and $V^{h,p}$ should be nearly orthogonal with respect to the inner product $B(\cdot,\cdot)$, in the sense that there is a constant $\gamma$, $0 \leq \gamma < 1$ such that the *strengthened Cauchy-Schwartz inequality* holds:

$$|B(v,w)| \leq \gamma \|v\|_e \|w\|_e, \qquad \forall v \in V^{h,p}, \quad \forall w \in W. \tag{4.22}$$

Finally, the lower bound can be improved by a recycling process (its cost is negligible when the finite element solution $u_{h,p}$ is solved using a direct method) as follows.

THEOREM 4.6. IMPROVED LOWER BOUND. *Let $\psi \in W$ be the solution of (4.20) and let $\phi \in V^{h,p}$ be the function which satisfies*

$$B(\phi, v) = -B(\psi, v), \qquad \forall v \in V^{h,p}. \tag{4.23}$$

*Then*

$$\|e\|_e = \left\|\mathcal{R}^u_{h,p}\right\|_* \geq \sqrt{\|\psi\|^2_e + \|\phi\|^2_e}. \tag{4.24}$$

PROOF. See [8,20]. ∎

We denote by $\eta^u_{\text{low}}$ the error estimate in the energy norm

$$\eta^u_{\text{low}} = \sqrt{\|\psi\|^2_e + \|\phi\|^2_e}, \tag{4.25}$$

which provides a guaranteed lower bound on $\|e\|_e$.

### 4.3. Bounds for the Goal-Oriented Error Estimation

We now construct the global bounds $\eta^-_{\text{low}}$, $\eta^-_{\text{upp}}$, $\eta^+_{\text{low}}$, and $\eta^+_{\text{upp}}$ introduced in Section 3.2. These are actually computed using the estimates $\psi^e$, $\phi^e$, and $\tilde{\varphi}^e_K$ with respect to the error $e$, solving (4.20), (4.23), and (4.16), respectively, and the estimates $\psi^\varepsilon$, $\phi^\varepsilon$, and $\tilde{\varphi}^\varepsilon_K$ with respect to $\varepsilon$, solving the same problems as before but using the residual $\mathcal{R}^w_{h,p}$ instead of $\mathcal{R}^u_{h,p}$. Observing that these problems are all linear, we then have the global lower bounds

$$\eta^-_{\text{low}} = \sqrt{\left\| s\,\psi^e - \frac{\psi^\varepsilon}{s} \right\|^2_e + \left\| s\,\phi^e - \frac{\phi^\varepsilon}{s} \right\|^2_e}, \tag{4.26}$$

$$\eta^+_{\text{low}} = \sqrt{\left\| s\,\psi^e + \frac{\psi^\varepsilon}{s} \right\|^2_e + \left\| s\,\phi^e + \frac{\phi^\varepsilon}{s} \right\|^2_e}, \tag{4.27}$$

and the global upper bounds

$$\eta^-_{\text{upp}} = \sqrt{\sum_K \left\| s\,\tilde{\varphi}^e_K - \frac{\tilde{\varphi}^\varepsilon_K}{s} \right\|^2_{e,K}}, \tag{4.28}$$

$$\eta^+_{\text{upp}} = \sqrt{\sum_K \left\| s\,\tilde{\varphi}^e_K + \frac{\tilde{\varphi}^\varepsilon_K}{s} \right\|^2_{e,K}}. \tag{4.29}$$

Moreover, the scaling factor $s$ in the expressions above is obtained by using either estimates of the global energy norms $\|e\|_e$ and $\|\varepsilon\|_e$.

## 5. ADAPTIVE CONTROL OF THE ERROR $L(e)$

The simplest strategy to control the approximation error consists in an iterative process whose steps are described below. This strategy is very general as it does not require any information about the type of problem. The algorithm is described in Figure 1.

1. Construct an initial coarse mesh in $\Omega$.
2. Compute the finite element solution $u_{h,p}$.
3. Compute an estimate of the error in a quantity of interest.
4. Check whether the relative error is smaller than a given preset tolerance $C^{\text{tol}}$. The iterative procedure terminates if the tolerance is reached.
5. If the tolerance is not achieved, adapt the finite element mesh in order to reduce the effects of the sources of errors, either by $h$-refinement or $p$-enrichment.
6. Go to Step 2.

Figure 1. Algorithm for error control.

We have seen in Section 3 an approach to estimate the error with respect to a bounded linear functional. In this case, the relative error is given by

$$e_{\text{rel}} = \frac{|L(e)|}{|L(u)|}. \tag{5.1}$$

Since both the exact solution and error are unknown, we use the available approximations instead. Then, the mesh needs to be adapted whenever

$$e_{\text{rel}} \approx \frac{|\eta^L|}{|L\,(u_{h,p})|} \geq C^{\text{tol}}, \tag{5.2}$$

where $\eta^L$ denotes an error estimate for $L(e)$. We note however that the relative error needs to be used with caution as the contributions to the quantity $L(u)$ may cancel out for nonzero $u$.

The objective in mesh adaptation is to refine the elements which exhibit large sources of error. In the present case, this simply means refining the elements which contribute the most to the quantity $L(e)$. This is made possible by decomposing the estimate $\eta^L$ into elementwise contributions. We may use, for example, equation (3.25) such that

$$\eta^L = \sum_K \eta_K^L = \sum_K \eta_K^u \eta_K^\omega. \tag{5.3}$$

Therefore, an element $\Omega_K$ of the mesh is refined if

$$\frac{\eta_K^L}{\max_J(\eta_J^L)} \geq C^{\text{adp}}. \tag{5.4}$$

Here, $C^{\text{adp}}$ is a user-defined parameter ranging between 0 and 1.

In the numerical experiments presented in the next section, meshes are made up of quadrilateral elements. The refinement procedure consists here in dividing an element into four subquadrilaterals, allowing for "hanging nodes", as shown in [17].

## 6. NUMERICAL EXAMPLE

We now illustrate the theory with examples. Numerical results were presented in [8] in the case of a two-point boundary value problem. We study here the case of two-dimensional boundary value problems.

In the following, we seek the solution of the Laplace equation on a square domain of unit size $\Omega = (0,1) \times (0,1)$,

$$-\Delta u = f, \qquad \text{in } \Omega, \tag{6.1}$$

which satisfies the boundary conditions

$$\begin{aligned} \frac{\partial u}{\partial n} &= 0, \qquad \text{on } x = 0, \quad x = 1, \quad y = 1, \\ u &= 0, \qquad \text{on } y = 0. \end{aligned}$$

The solution of this class of problems belongs to the space $V = \{v \in H^1(\Omega); v = 0 \text{ on } y = 0\}$ for sufficiently smooth $f$. Here, we consider the particular problem where the exact solution $u$ is given by the function

$$u(x,y) = 5\, x^2 (1-x)^2 \left(e^{10x^2} - 1\right)\, y^2 (1-y)^2 \left(e^{10y^2} - 1\right), \tag{6.2}$$

which is plotted in Figure 2. We observe that the solution possesses a symmetry with respect to the line $x = y$, but the problem itself is not symmetric because of the particular choice of boundary conditions. As a consequence, the adapted meshes will not necessarily show this symmetry.

In all experiments, the domain is initially discretized into a uniform mesh of 64 elements as shown in Figure 3. The polynomial degree $p$ for the approximation $u$ is uniformly set to one in all cases. Moreover, we select $q = 2$ in all elements so that the bubble functions of $W$ are the basis functions of degree $p = 2$ and 3.

In the first series of experiments, we briefly study the global error estimators $\eta_{\text{low}}^u$ and $\eta_{\text{upp}}^u$. As usual, we measure the quality of the estimators with the effectivity index

$$\lambda = \frac{\eta^u}{\|e\|_e}, \tag{6.3}$$

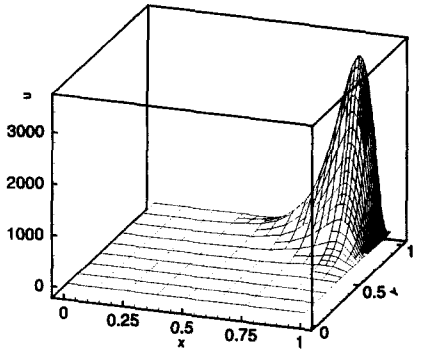


Figure 2. Exact solution.

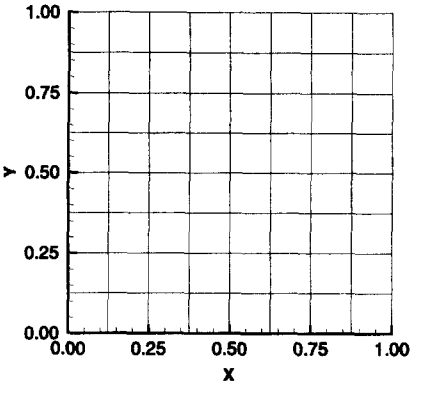


Figure 3. Initial mesh.

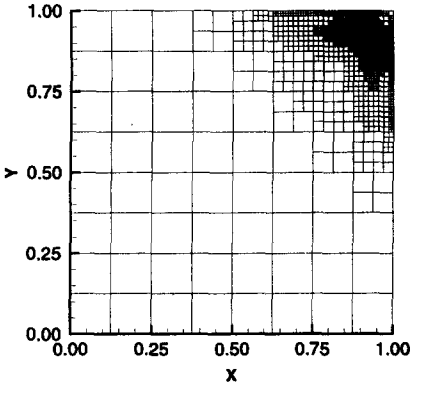


Figure 4. Adapted mesh based on the global error estimator.

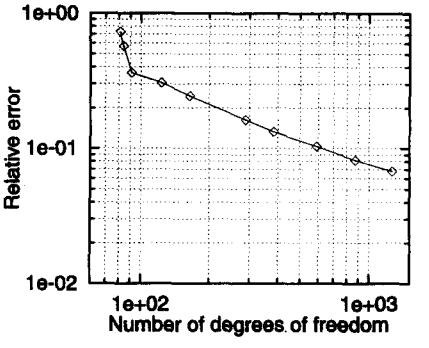


Figure 5. Relative error for global mesh adaptation.

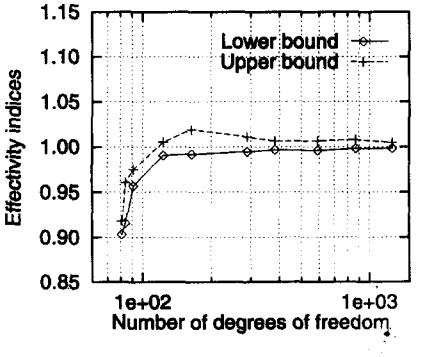


Figure 6. Effectivity indices of lower and upper bounds in energy norm.

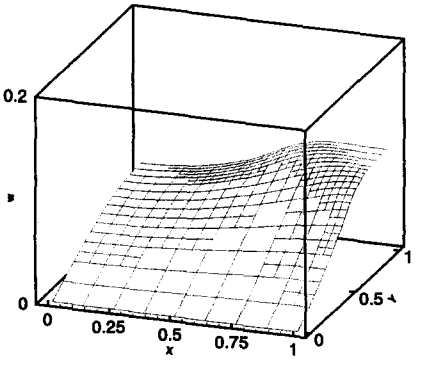


Figure 7. Influence function associated with the average of $u$ in $\Omega_s$.

where $\eta^u$ refers either to $\eta^u_{\text{low}}$ or to $\eta^u_{\text{upp}}$. The error estimators are tested on a sequence of meshes obtained by global adaptive refinement, the final mesh being shown in Figure 4 and containing 1261 elements. As expected and shown in Figure 5, the relative error in the asymptotic range exhibits a first-order convergence rate (indeed, using the last two points in the graph of the relative error, we obtain $e_{\text{rel}} = 1.03\mathcal{O}(N_{\text{dof}}^{1/2})$ where $N_{\text{dof}}$ denotes the total number of degrees of freedom).

The effectivity indices for the lower- and upper-bound estimates with respect to the number of degrees of freedom are shown in Figure 6. We observe that both estimates provide effectivity

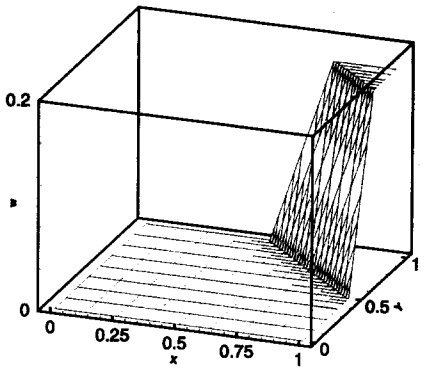


Figure 8. Influence function associated with the average of $\mathbf{n}\nabla u$ in $\Omega_s$.

indices close to one, but $\eta^u_{\text{upp}}$ fails to provide an upper bound to the exact error when the number of degrees of freedom is small. However, we notice that $\eta^u_{\text{low}}$ is always smaller than $\eta^u_{\text{upp}}$.

### 6.1. Goal-Oriented Error Estimation: Average of Solution

In this section, we study the performance of the error estimates with respect to the average of the solution in a subdomain of $\Omega$. We suppose here that we are interested in the average of $u$ over the subdomain $\Omega_s$ defined as

$$\Omega_s = \Omega \cap \{(x, y);\ 1.5 < x + y < 1.75\}. \tag{6.4}$$

This subdomain corresponds to the strip in the right upper corner of the domain as shown in Figure 9. The linear functional $L(u)$ for this example is defined as in (3.27). We show in Figure 7 an accurate approximation of the influence function $\omega$ obtained by adaptive mesh refinement based on the global error in $\omega$. We also show, in Figure 8, the influence function corresponding to the average of the directional derivative $\mathbf{n}\nabla u$ in $\Omega_s$, where $\mathbf{n} = (\sqrt{2}/2, \sqrt{2}/2)$.

Next, we test the adaptive strategy with respect to our quantity of interest. We show in Figure 9 an intermediate mesh (169 elements) and the final mesh (661 elements) for which the relative error

$$e_{\text{rel}} = \frac{|L(e)|}{|L(u)|} \tag{6.5}$$

is less than 0.1 percent. We note that the exact value $L(u)$ is equal to 832.04, so that the error in average on $\Omega_s$ has been reduced to less than one. We observe that the final mesh has been refined in $\Omega_s$, but also in the upper corner where there exist large sources of error. Moreover, we infer from Figure 10, showing the evolution of the relative error $e_{\text{rel}}$ versus the number of degrees of freedom, that the goal-oriented adaptive strategy does indeed improve the rate of convergence in relation to the global adaptive strategy.

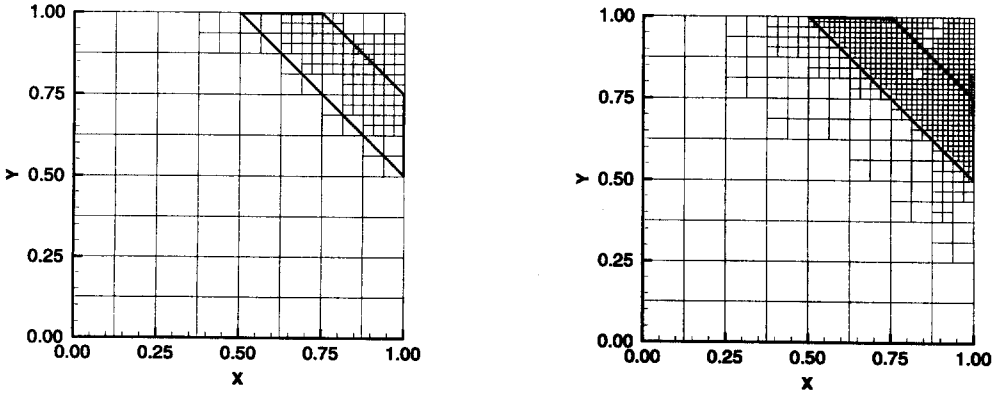


Figure 9. Adapted meshes, intermediate and final, to control the average of $u$ in $\Omega_s$.

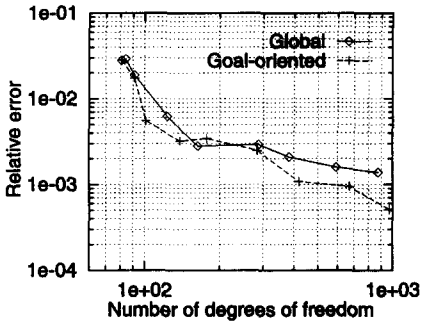


Figure 10. Comparison of the relative error for the average of $u$ in $\Omega_s$.

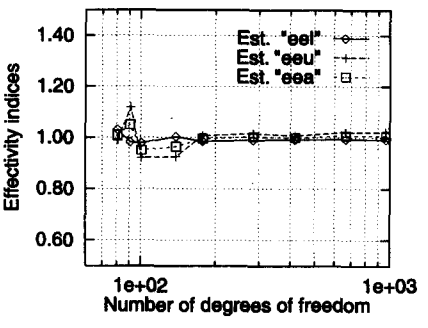


Figure 11. Effectivity indices of $\eta^L_{\text{eel}}$, $\eta^L_{\text{eeu}}$, and $\eta^L_{\text{eea}}$ for the average of $u$ in $\Omega_s$.

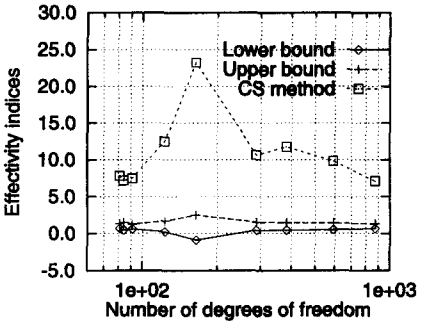


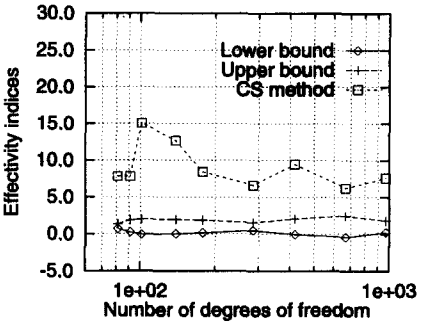


Figure 12. Effectivity indices of $\eta^L_{\text{low}}$, $\eta^L_{\text{upp}}$, and $\eta^L_{\text{cs}}$ for the average of $u$ in $\Omega_s$ on a sequence of meshes obtained by global (left) and goal-oriented (right) refinement.

We finally study the error estimates $\eta^L_{\text{eel}}$, $\eta^L_{\text{eeu}}$, and $\eta^L_{\text{eea}}$ and bounds $\eta^L_{\text{low}}$, $\eta^L_{\text{upp}}$, and $\eta^L_{\text{cs}}$ in relation with the quantity $L(e)$. In this case, the effectivity indices read

$$\lambda = \frac{\eta^L}{L(e)}, \tag{6.6}$$

where $\eta^L$ refers to each of the estimates and bounds. In Figure 11, we show the effectivity indices of the estimates computed on a sequence of meshes obtained by goal-oriented refinement. All three estimates provide indices close to one whatever the level of refinement. Following Remark 3.1, we expect the results for the bounds $\eta^L_{\text{low}}$ and $\eta^L_{\text{upp}}$ to be different whether we use global or goal-oriented refinements. Surprisingly, the effectivity of the lower and upper bounds does not exceed $-1$ and $+3$, respectively, in both cases. We also observe in Figure 12 that the bound $\eta^L_{\text{cs}}$ is less accurate by a factor up to ten.

### 6.2. Goal-Oriented Error Estimation: Pointwise Value

The next set of experiments is devoted to the study of pointwise error estimation applying the methodology proposed in Section 3.4. The goal is then represented by the bounded linear functional $L(u)$ defined in (3.34). We choose here two points, $\mathbf{x}_{01}$ and $\mathbf{x}_{02}$, in $\Omega$. The first is given by the coordinates $\mathbf{x}_{01} = (0.8, 0.65)$ and is situated in the lower part of the "bump" featured by the solution as shown in Figure 2. The second is chosen away from the "bump" at the coordinates $\mathbf{x}_{02} = (0.6, 0.4)$ in order to analyze the effect of "pollution" (i.e., the effect of far-field residuals).

The influence functions associated with the points $\mathbf{x}_{01}$ and $\mathbf{x}_{02}$ are shown in Figures 13 and 14, respectively. These were approximated by setting the parameter $\epsilon$ in the mollifying kernel $k_\epsilon$ to $\epsilon = 0.001$. We remark that the influence functions would converge to the corresponding Green functions when $\epsilon$ tends to zero.

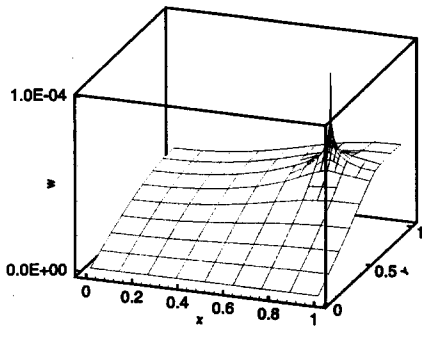


Figure 13. Influence function associated with pointwise solution at $\mathbf{x}_{01}$.

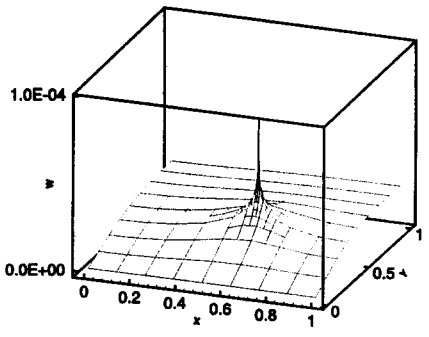


Figure 14. Influence function associated with pointwise solution at $\mathbf{x}_{02}$.

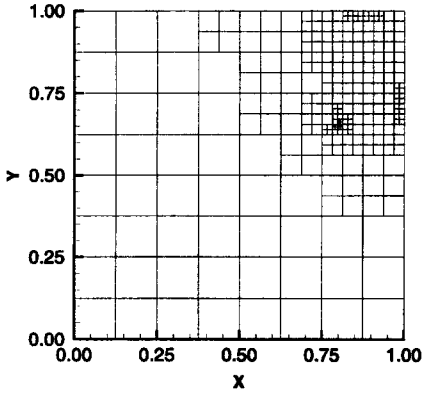


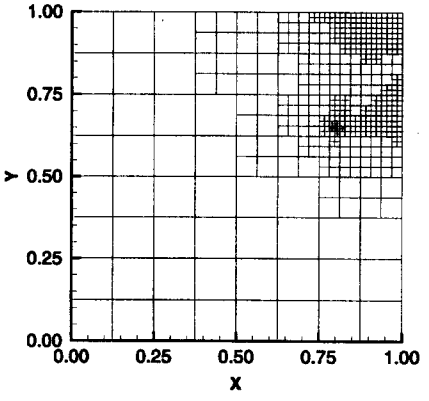


Figure 15. Adapted meshes, intermediate and final, based on pointwise error estimate at $\mathbf{x}_{01}$.

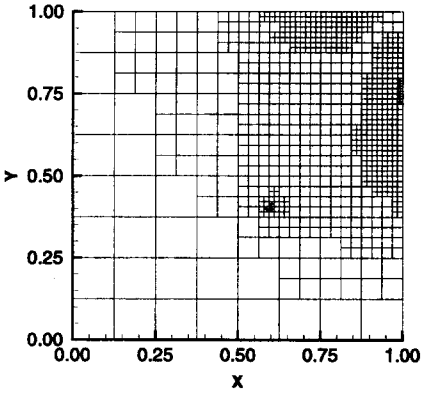


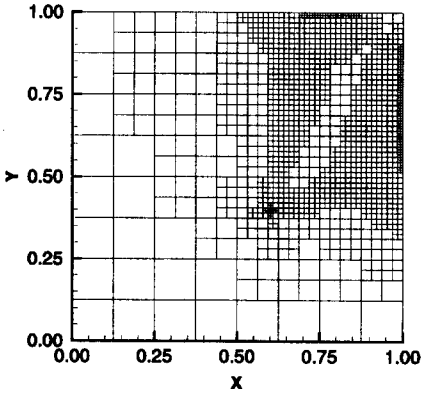


Figure 16. Adapted meshes, intermediate and final, based on pointwise error estimate at $\mathbf{x}_{02}$.

Next, we test the adaptive strategy for the control of the pointwise error. Our first objective is to predict the solution $u$ at $\mathbf{x}_{01}$ within the tolerance $C^{\text{tol}} = 0.5$ percent. The adapted meshes, one intermediate (271 elements) and the final one (472 elements), are shown in Figure 15. On the final mesh, we obtain $L(u_{h,p}) = 268.52$, whereas the exact value is $u(\mathbf{x}_{01}) = 268.18$. The relative error is then about 0.13 percent. The second objective was to predict $u(\mathbf{x}_{02})$ within $C^{\text{tol}} = 6$ percent. We show an intermediate mesh (799 elements) and the final mesh (1351 elements) in Figure 16. Actually, the predicted value is $L(u_{h,p}) = 2.46$, the exact value $u(\mathbf{x}_{02}) = 2.33$, and the relative error about 5.6 percent. We observe that the computation is more demanding for $\mathbf{x}_{02}$ than for $\mathbf{x}_{01}$. This is due to the fact that $u(\mathbf{x}_{02}) \ll u(\mathbf{x}_{01}) < \max_{\Omega}(u)$ in this example. This implies that the

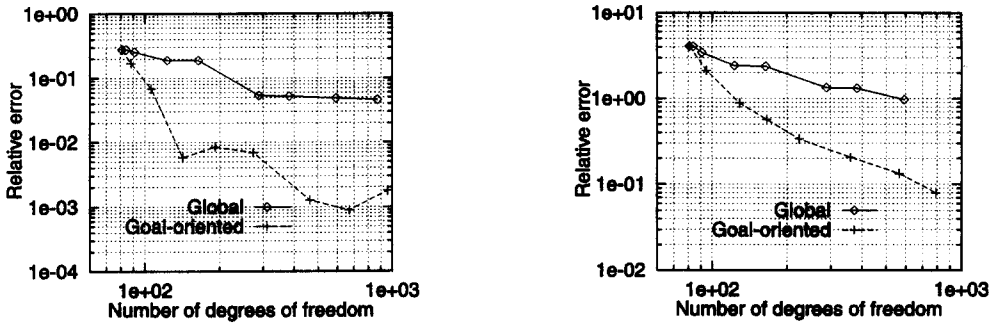


Figure 17. Comparison of the relative error $e_{\text{rel}}$ using the global and goal-oriented adaptivity strategies for $\mathbf{x}_{01}$ (left) and $\mathbf{x}_{02}$ (right).

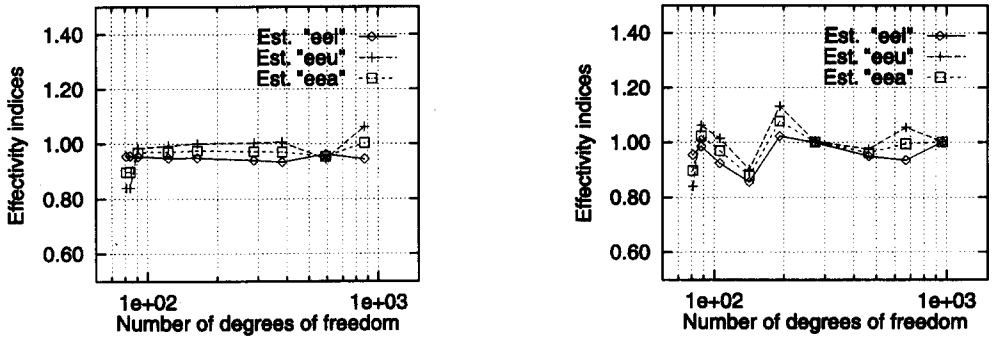


Figure 18. Effectivity indices of $\eta^L_{\text{eel}}$, $\eta^L_{\text{eeu}}$, and $\eta^L_{\text{eea}}$ for the pointwise error at $\mathbf{x}_{01}$ on a sequence of meshes obtained by global (left) and goal-oriented (right) refinement.

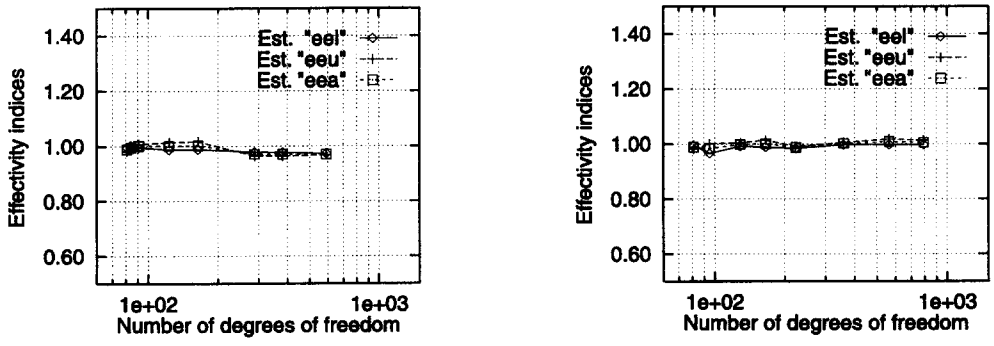


Figure 19. Effectivity indices of $\eta^L_{\text{eel}}$, $\eta^L_{\text{eeu}}$, and $\eta^L_{\text{eea}}$ for the pointwise error at $\mathbf{x}_{02}$ on a sequence of meshes obtained by global (left) and goal-oriented (right) refinement.

error at $\mathbf{x}_{02}$ is expected to be influenced by remote sources of errors, and indeed, the final mesh for the point $\mathbf{x}_{02}$ is refined in a broader region than the final mesh for $\mathbf{x}_{01}$. Here, since we are interested in the pointwise error and since the exact value $u(\mathbf{x}_0)$ is continuous and nonzero at $\mathbf{x}_0 = \mathbf{x}_{01}$ and $\mathbf{x}_{02}$, we define the relative error as

$$e_{\text{rel}} = \frac{|u(\mathbf{x}_0) - L(u_{h,p})|}{|u(\mathbf{x}_0)|}. \tag{6.7}$$

We compare in Figure 17 the relative error $e_{\text{rel}}$ with respect to the number of degrees of freedom when we utilize the adaptive strategies based on either the global estimator in the energy norm or the estimator in the goal of interest. We observe that the rate of convergence with respect to our goal, here the pointwise value, is dramatically improved, by about one to two orders of magnitude, when using the latter strategy. We also remark that the rate of convergence is not necessarily monotonic.

We finally investigate the performance of the estimates $\eta^L_{\text{eel}}$, $\eta^L_{\text{eeu}}$, and $\eta^L_{\text{eea}}$ and bounds $\eta^L_{\text{low}}$, $\eta^L_{\text{upp}}$, and $\eta^L_{\text{cs}}$. Here, the effectivity index is given with respect to the exact pointwise error at $\mathbf{x}_0$ when it is nonzero

$$\lambda = \frac{\eta^L}{e(\mathbf{x}_0)}. \tag{6.8}$$

We compare the accuracy of the estimates on sequences of meshes obtained by global or goal-oriented adaptivity. The results are shown in Figure 18 for $\mathbf{x}_{01}$ and in Figure 19 for $\mathbf{x}_{02}$. We observe that in all cases, the effectivity indices of the three estimates are very close to one but that none of them consistently provides better results than the others.

We show in Figures 20 and 21 the effectivity indices of the bounds for $\mathbf{x}_{01}$ and $\mathbf{x}_{02}$, respectively. This time, the effectivity indices of $\eta^L_{\text{low}}$ and $\eta^L_{\text{upp}}$ vary between $-8$ and 10 when the mesh is adapted with respect to the energy norm of the error. However, when the mesh is adapted according to the goal, the bounds take on much larger values and have the tendency to diverge as the number of degrees of freedom increase. This behavior was actually expected in view of Remark 3.1. On the other hand, the bound $\eta^L_{\text{cs}}$ provides consistent results, but is not guaranteed to be better than $\eta^L_{\text{low}}$ or $\eta^L_{\text{upp}}$. We remark that the bound $\eta^L_{\text{cs}}$ is computed here using $\eta^u_{\text{low}}$ and $\eta^\omega_{\text{low}}$.

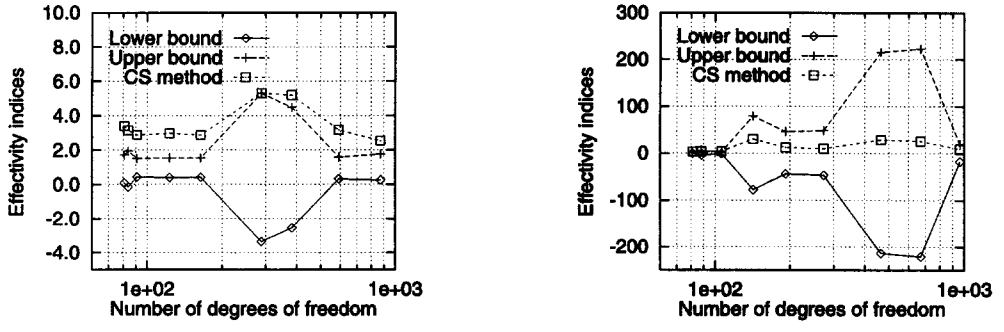


Figure 20. Effectivity indices of $\eta^L_{\text{low}}$, $\eta^L_{\text{upp}}$, and $\eta^L_{\text{cs}}$ for the pointwise error at $\mathbf{x}_{01}$ on a sequence of meshes obtained by global (left) and goal-oriented (right) refinement.

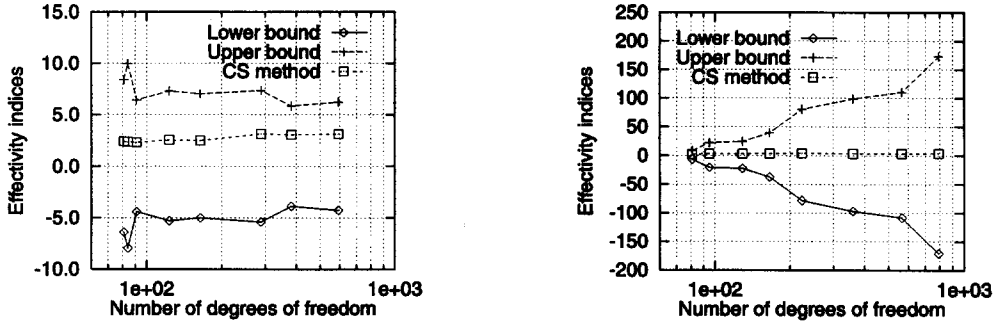


Figure 21. Effectivity indices of $\eta^L_{\text{low}}$, $\eta^L_{\text{upp}}$, and $\eta^L_{\text{cs}}$ for the pointwise error at $\mathbf{x}_{02}$ on a sequence of meshes obtained by global (left) and goal-oriented (right) refinement.

### 6.3. Goal-Oriented Error Estimation: Pointwise Directional Derivative

We repeat the previous experiments for the pointwise derivative $\mathbf{n}\nabla u$ at the point $\mathbf{x}_{03} = (0.65, 0.65)$ in the direction $\mathbf{n} = (\sqrt{2}/2, \sqrt{2}/2)$. In this case, the linear functional associated with this quantity of interest is given in (3.38).

We show in Figure 22 the corresponding influence function and in Figure 23 examples of adapted meshes. The intermediate mesh contains 307 elements and the final one 748 elements. The relative error on the final mesh is about 0.7 percent whereas $\mathbf{n}\nabla u(\mathbf{x}_{03}) = 907.50$.

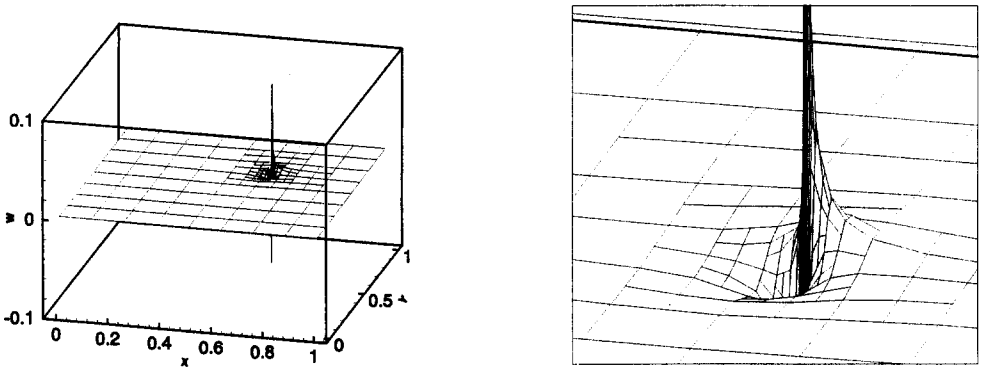


Figure 22. Influence function associated with the pointwise derivative $\mathbf{n}\nabla u$ at $\mathbf{x}_{03}$ in the direction $\mathbf{n} = (\sqrt{2}/2, \sqrt{2}/2)$.

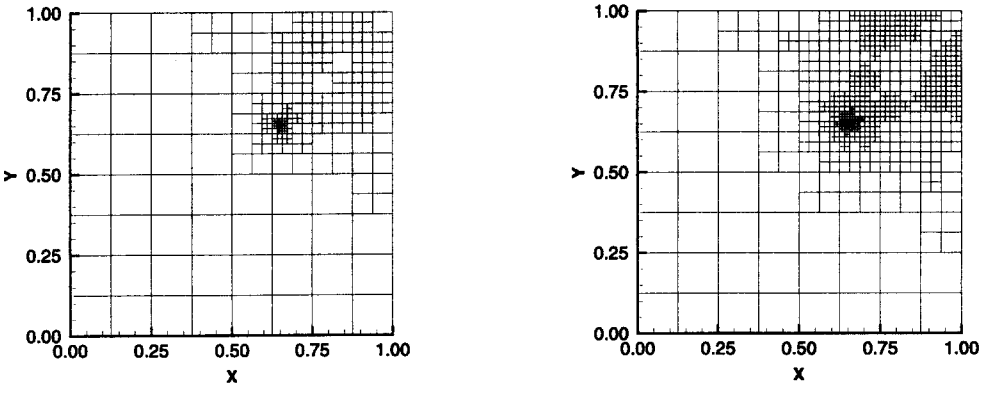


Figure 23. Adapted meshes, intermediate and final, to control the pointwise directional derivative at $\mathbf{x}_{03}$.

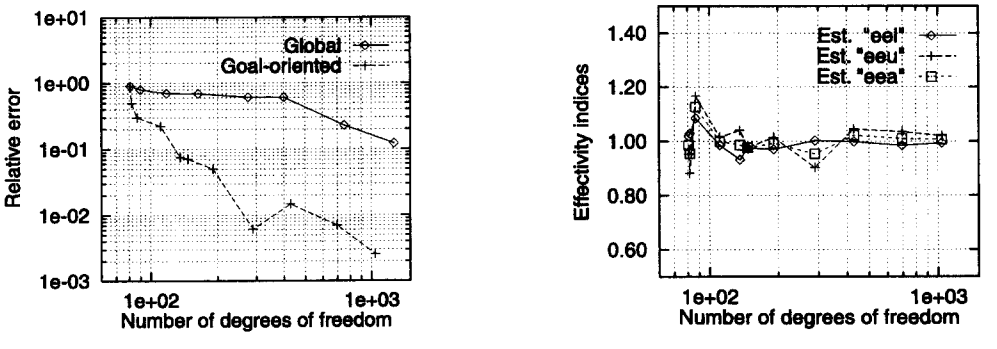


Figure 24. Comparison of the relative error for the pointwise directional derivative.

Figure 25. Effectivity indices of $\eta^L_{\text{eel}}$, $\eta^L_{\text{eeu}}$, and $\eta^L_{\text{eea}}$ for the pointwise directional derivative.

We also show the evolution of the relative error in Figure 24 and the effectivity indices of $\eta^L_{\text{eel}}$, $\eta^L_{\text{eeu}}$, and $\eta^L_{\text{eea}}$ in the case of adapted meshes based on the goal-oriented strategy in Figure 25. Then we show the effectivity of the bounds in Figure 26. The bounds $\eta^L_{\text{low}}$ and $\eta^L_{\text{upp}}$ are not represented for the case of goal-oriented adapted meshes as their effectivity index becomes too large (greater than $\pm 10^3$).

## 7. CONCLUSIONS

The numerical examples presented in this paper verify the goal-oriented error estimates and suggest that goal-oriented mesh adaptivity can greatly accelerate the calculation of quantities

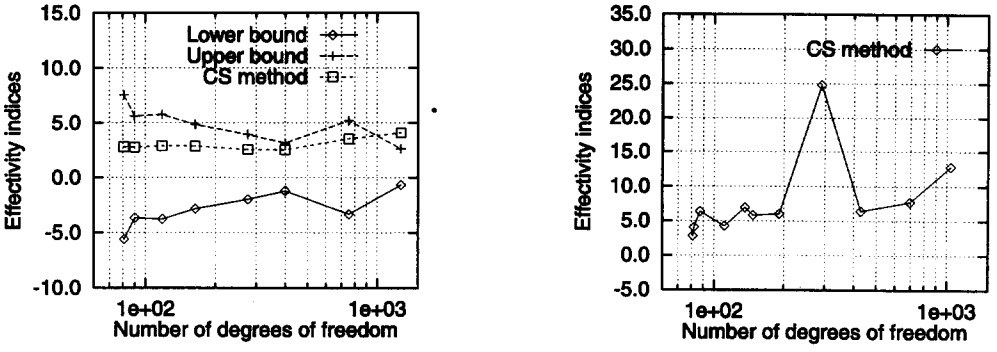


Figure 26. Effectivity indices of the bounds $\eta^L_{\text{low}}$, $\eta^L_{\text{upp}}$, and $\eta^L_{\text{cs}}$ for the error in the pointwise directional derivative on a sequence of meshes obtained by global (left) or goal-oriented (right) refinement.

of interest to preset levels of accuracy. In particular, the rate of convergence of goal-oriented adaptive procedures is greatly accelerated compared to traditional adaptive schemes based on global energy estimates for a class of model test problems. The experiments also show that the estimates for these problems are excellent as their effectivity indices are all close to one. However, the quality of the bounds on the error are understandably sensitive to the quality of the error estimates in the energy norm and on the quantity of interest itself. The reliability of these bounds could be improved by improving the effectivity indices of the global energy estimates.

## REFERENCES

1. R. Becker and R. Rannacher, Weighted *a posteriori* error control in FE method, *ENUMATH-95, Paris*, (September 1995).
2. R. Becker and R. Rannacher, A feedback approach to error control in finite elements methods: Basic analysis and examples, Preprint 96-52, Institut für Angewandte Mathematik, Universität Heidelberg, (1996).
3. R. Rannacher and F.T. Stuttmeier, *A posteriori* error control in finite element methods via duality techniques: Application to perfect elasticity, Preprint 97-16, Institut für Angewandte Mathematik, Universität Heidelberg, (1997).
4. F. Cirak and E. Ramm, *A posteriori* error estimation and adaptivity for linear elasticity using the reciprocal theorem, *Comp. Meth. in Appl. Mech. and Eng.* **156**, 351–362, (1998).
5. M. Paraschivoiu and A.T. Patera, A hierarchical duality approach to bounds for the outputs of partial differential equations, *Comp. Meth. in Appl. Mech. and Eng.* **158**, 389–407, (1998).
6. J. Peraire and A.T. Patera, Bounds for linear-functional outputs of coercive partial differential equations: Local indicators and adaptive refinement, In *Advances in Adaptive Computational Methods in Mechanics*, (Edited by P. Ladevèze and J.T. Oden), pp. 199–215, Elsevier, Amsterdam, (1998).
7. I. Babuška, T. Strouboulis, K. Copps, S.K. Gangaraj and C.S. Upadhyay, *A posteriori* error estimation for finite element and generalized finite element method, TICAM Report 98-01, The University of Texas at Austin, (1998).
8. S. Prudhomme and J.T. Oden, On goal-oriented error estimation for elliptic problems: Application to the control of pointwise errors, *Comp. Meth. in Appl. Mech. and Eng.* (to appear).
9. M. Ainsworth and J.T. Oden, A unified approach to *a posteriori* error estimation using element residual methods, *Numer. Math.* **65** (1), 23–50, (1993).
10. M. Ainsworth and J.T. Oden, *A posteriori* error estimation in finite element analysis, *Comp. Meth. in Appl. Mech. and Eng.* **142**, 1–88, (1997).
11. I. Babuška and W. Rheinboldt, *A posteriori* error estimates for the finite element method, *Int. J. Numer. Methods Eng.* **12**, 1597–1615, (1978).
12. R.E. Bank and A. Weiser, Some *a posteriori* error estimators for elliptic partial differential equations, *Math. Comp.* **44**, 283–301, (1985).
13. R.E. Bank and R.K. Smith, *A posteriori* error estimates based on hierarchical bases, *SIAM J. Numer. Anal.* **30** (4), 921–935, (1993).
14. R. Verfürth, *A Review of A Posteriori Error Estimation and Adaptive Mesh-Refinement Techniques*, Wiley-Teubner, Stuttgart, (1996).
15. O.C. Zienkiewicz and J.Z. Zhu, The superconvergent patch recovery and *a posteriori* error estimates. Part 1: The recovery technique, *Int. J. Numer. Methods Eng.* **33**, 1331–1364, (1992).
16. O.C. Zienkiewicz and J.Z. Zhu, The superconvergent patch recovery and *a posteriori* error estimates. Part 2: Error estimates and adaptivity, *Int. J. Numer. Methods Eng.* **33**, 1365–1382, (1992).

17. L. Demkowicz, J.T. Oden, W. Rachowicz and O. Hardy, Toward a universal $h$-$p$ adaptive finite element strategy. Part 1. Constrained approximation and data structure, *Comp. Meth. in Appl. Mech. and Eng.* **77**, 113–180, (1989).
18. J.T. Oden and G.F. Carey, *Finite Elements: Mathematical Aspects, Volume IV*, Prentice-Hall, (1983).
19. J.T. Oden and J.N. Reddy, *An Introduction to the Mathematical Theory of Finite Elements*, John Wiley & Sons, New York, (1976).
20. S. Prudhomme, Adaptive control of error and stability of $h$-$p$ approximations of the transient Navier-Stokes equations, Ph.D. Thesis, The University of Texas at Austin, (1999).